Engineering with Computers (2020) 36:359–375
https://doi.org/10.1007/s00366-019-00703-6

ORIGINAL ARTICLE

Develop a refined truncated cubic lattice structure for nonlinear large-amplitude vibrations of micro/nano-beams made of nanoporous materials

S. Sahmani[1] · A. M. Fattahi[2] · N. A. Ahmed[2]

Received: 13 April 2018 / Accepted: 6 January 2019 / Published online: 28 January 2019

Abstract
Pore size and interconnectivity have essential role in different biological applications of synthetic porous biomaterials. Recent improvements in technology make it possible to produce nanoporous materials having pores of controllable dimensions at atomic scale. In the present study, based upon a refined truncated cube lattice structure, the elastic mechanical properties of nanoporous materials have been extracted explicitly in terms of the pore size. Afterwards, the size-dependent nonlinear large-amplitude vibrations of micro/nano-beams made of the nanoporous material are explored. To this purpose, the nonlocal strain gradient elasticity theory is utilized within the framework of the refined hyperbolic shear deformation beam theory to capture the both small-scale effects of hardening-stiffness and softening-stiffness. Finally, the Galerkin method together with an improved perturbation technique is employed to construct explicit analytical expression for the nonlocal strain gradient frequency-deflection response of micro/nano-beams made of nanoporous materials. It is demonstrated that, by increasing the pore size, the nonlinear frequency associated with the large-amplitude vibration of micro/nano-beams made of nanoporous material reduces, but the rate of this reduction becomes lower for higher pore size.

Keywords Nano-technology · Porous materials · Size effect · Nonlinear vibration · Perturbation technique

1 Introduction

Different reasons such as diseases, trauma, congenital defects, etc. may lead to the degeneration of tissues in the human body. Nowadays, via development in tissue engineering, novel approaches have been emerged to regenerate a damaged tissue, in spite of replacing it. In this way, pore architecture and porosity of scaffolds play an essential role in cell migration and in growth, and recently, several studies have been performed in this research area. Shariful Islam and Todo [1] discovered the sintering effects on the compressive mechanical properties of the scaffold. Hedayati et al. [2] analyzed the fatigue crack propagation in additively manufactured porous biomaterial via an analytical model. Zhang et al. [3] investigated the influence of three kinds of sterilization methods on a porous zein scaffold as a new biomaterial. Bobbert et al. [4] designed porous metallic biomaterials on the basis of four different types of triply periodic minimal surfaces which cause to mimic the properties of bone to an unprecedented level. Kadkhodapour et al. [5] utilized triply periodic minimal surfaces to obtain structure–property relations for Ti6Al4V scaffolds designed.

Nanoscale porous biomaterials have been recently evolved as a new class of porous materials having exciting applications. For instance, the materials utilized to manufacture nanoscaffolds in heart valves are typically packed together with pores of a very small size to direct the colonization and growth of cells in a more efficient way. Due to high surface-to-volume ratio as well as size-dependent characteristics, nanoporous materials feature unique behavior in comparison with the conventional porous materials [6].

To make the continuum mechanical applicable in the analysis of micro/nano-structures, it needs to take small-length

✉ S. Sahmani
ssahmani@nri.ac.ir; sahmani@aut.ac.ir

✉ A. M. Fattahi
afattahi@uj.ac.za

1 Mechanical Rotating Equipment Department, Niroo Research Institute (NRI), Tehran 14665-517, Iran

2 Mechanical Engineering Science Department, Faculty of Engineering and Built Environment, University of Johannesburg, Johannesburg 2006, South Africa

scales such as lattice spacing and grain size into account. Up to now, various unconventional continuum theories have been established to consider size dependence in mechanical characteristics of micro/nano-structures [7–40]. Recently, it is indicated that nonlocal differential model is an approximate model and may be not equivalent to integral elasticity based model [41, 42,42]. According to the previous studies, it has been observed that the nonlocal elasticity theory and strain gradient continuum mechanics represent two entirely different size effects including softening-stiffness and hardening-stiffness influences.

To overcome this paradox, Lim et al. [43] developed the nonlocal strain gradient elasticity theory which incorporates simultaneously the both features of size dependence. After that, several investigations have been carried out to analyze size-dependent mechanical behavior of micro/nano-structures. Li and Hu [10] used the nonlocal strain gradient theory of elasticity to develop a size-dependent Euler–Bernoulli beam model for buckling analysis of nano-beams. They also formulated the equations related to the wave motion fluid-conveying viscoelastic carbon nano-tubes based upon the nonlocal strain gradient continuum mechanics [44]. Simsek [14] examined the size-dependent nonlinear vibrations of functionally graded Euler–Bernoulli nano-beams via nonlocal strain gradient theory of elasticity. Li et al. [45] constructed a nonlocal strain gradient functionally graded Timoshenko beam model to analyze free vibration response of nano-beams. Yang et al. [46] studied the nonlocal strain gradient dynamic pull-in instability of functionally graded carbon nano-tube-reinforced nano-actuators. Li et al. [47] analyzed the longitudinal vibrations of nano-scaled rods on the basis of the nonlocal strain gradient elasticity theory. Tang et al. [17] predicted the viscoelastic wave propagation in an embedded viscoelastic carbon nano-tube based on the theory of nonlocal strain gradient elasticity. Sahmani and Aghdam [48–51] anticipated size-dependent nonlinear mechanical responses of multilayer functionally graded micro/nano-structures reinforced with graphene nanoplatelets based on the nonlocal strain gradient continuum mechanics. Li and Hu [52] derived a nonlocal strain gradient model to study the postbuckling behavior of functionally graded nano-beams. Xu et al. [53] explored the nonlocal strain gradient bending and buckling of Euler–Bernoulli nano-beams. Based on the weighted residual approaches, Shahsavari et al. [54] analyzed damped vibration of a graphene sheet on the basis of a higher order nonlocal strain gradient plate model. Sahmani and Aghdam [55–58] captured size effects on the nonlinear instability of axially loaded and hydrostatic pressurized microtubules surrounded by cytoplasm based upon the nonlocal strain gradient shell model. Lu et al. [59] proposed a nonlocal strain gradient sinusoidal shear deformable beam model for the vibration analysis of nano-beams. Radic [60] investigated the size-dependent buckling behavior of porous double-layered functionally graded nanoplates resting on an elastic foundation via the nonlocal strain gradient theory of elasticity. Sahmani et al. [61–63] applied the nonlocal strain gradient elasticity to the classical continuum mechanics to capture size effects on nonlinear mechanical characteristics of functionally graded porous micro/nano-structures. Zhen et al. [64] explored the nonlocal strain gradient free vibration response of viscoelastic nano-tubes subjected to the longitudinal magnetic field. Sahmani and Khandan [65] analyzed the size-dependent nonlinear instability of magneto-electro-elastic cylindrical composite nanopanels within the framework of the nonlocal strain gradient panel model. Sahmani et al. [66] presented an analytical mathematical solution for vibration response of an axially loaded multilayer functionally graded micro/nano-beam reinforced with graphene platelets within both of the prebuckling and postbuckling domains. Lu et al. [67] developed a unified size-dependent plate model based upon the nonlocal strain gradient and surface stress elasticity theories for buckling analysis of nanoplates. Esfahani et al. [68] performed a nonlinear vibration analysis of an electrostatic nano-beam resonator on the basis of the nonlocal strain gradient continuum elasticity.

In the present investigation, at first, a refined form of the analytical approach developed by Hedayati et al. [69] is put to use to construct explicit expression for mechanical properties of nanoporous material made from refined truncated cube lattice structure in terms of pore size. Thereafter, based upon the extracted mechanical properties, the nonlocal strain gradient elasticity theory is utilized to capture two entirely different size dependencies in the nonlinear large-amplitude vibrations of micro/nano-beams made of the nanoporous material. The Galerkin method together with an improved perturbation technique is employed to achieve explicit analytical expression for nonlocal strain gradient frequency-deflection response of the nonlinear large-amplitude vibrations of micro/nano-beams made of nanoporous material.

2 Analytical approach for mechanical properties of nanoporous materials

In the present investigation, it is assumed that a nanoporous material is made from the refined truncated cube lattice structure including open cell foam which consists of bigger truncated cube cells and smaller tetrahedral cells, as illustrated in Fig. 1. Accordingly, by repeating the cells, a unit cell surrounding by the truncated cubes is resulted in, each membrane of which is dedicated to a unique refined truncated cube. It is demonstrated in Fig. 2 that, because of the geometrical symmetry, the links $c_1a_1b_1d_1a_2c_2$ and $c_1a_1b_2d_2a_2c_2$ and $c_1a_1b_3d_3a_2c_2$ and $c_1a_1b_4d_4a_2c_2$ of the unit cell have the same mechanical in-plane deformations.

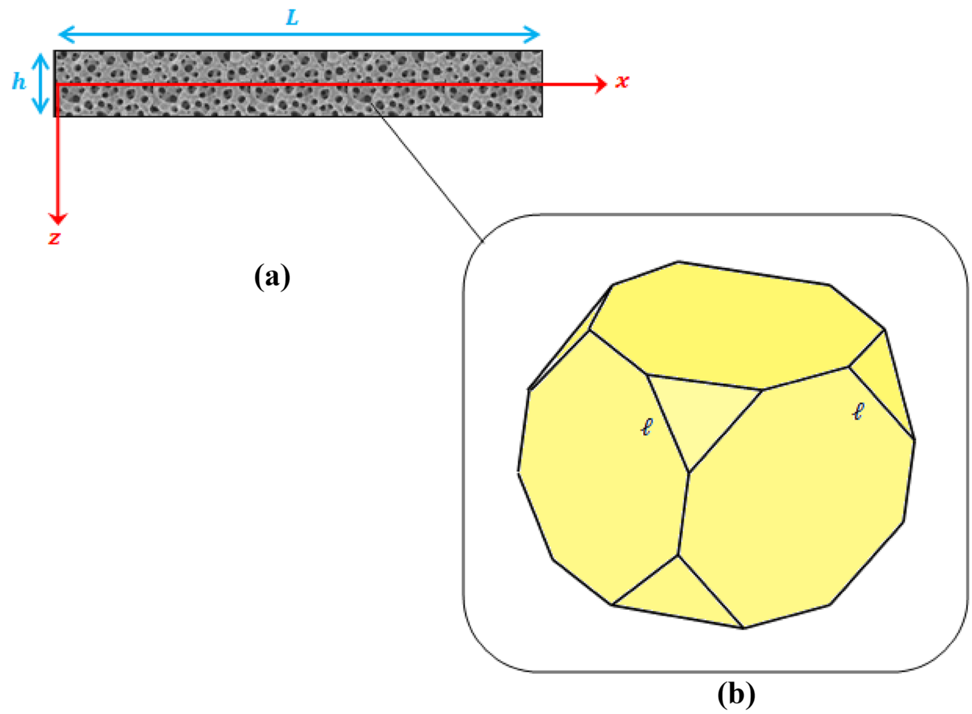

Fig. 1 A micro/nano-beam made of a nanoporous material: **a** coordinate system and geometric parameters; **b** a refined truncated cube lattice framework

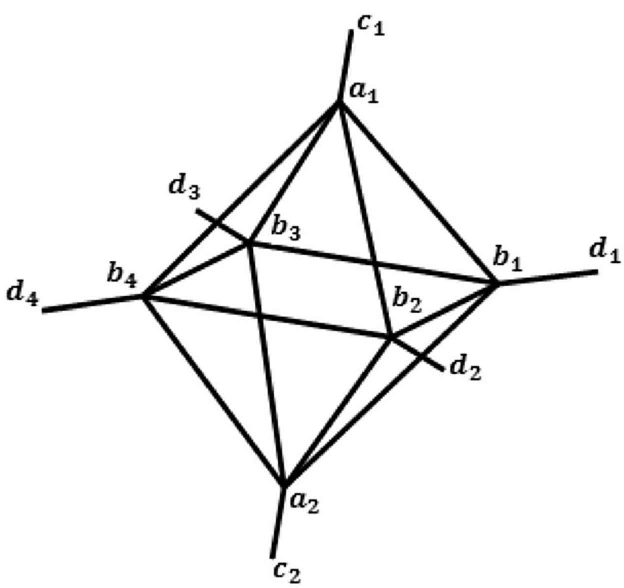

Fig. 2 A refined truncated cube unit cell

Consequently, analyzing one of them is enough to obtain the mechanical response of the unit cell. Here, the link $c_1a_1b_1d_1a_2c_2$ is chosen to be analyzed.

At first, on the basis of the refined hyperbolic shear deformable beam model for the links of the unit cell, one will have

$$\bar{E}\bar{I}\,\frac{d^4w}{dx^4} = \bar{E}\bar{I}\left[\cosh\left(\frac{1}{2}\right) - 12\left(\cosh\left(\frac{1}{2}\right) - 2\sinh\left(\frac{1}{2}\right)\right)\right]\frac{d^3\psi}{dx^3} + q(x), \tag{1a}$$

$$\bar{E}\bar{I}\left[\cosh\left(\frac{1}{2}\right) - 12\left(\cosh\left(\frac{1}{2}\right) - 2\sinh\left(\frac{1}{2}\right)\right)\right]\frac{d^3w}{dx^3} = \bar{E}\bar{I}\left[\left(\cosh\left(\frac{1}{2}\right)\right)^2 + 6(\sinh(1) - 1) - 24\cosh\left(\frac{1}{2}\right)\left(\cosh\left(\frac{1}{2}\right) - 2\sinh\left(\frac{1}{2}\right)\right)\right]\frac{d^2\psi}{dx^2} - \bar{G}\bar{A}\left[\left(\cosh\left(\frac{1}{2}\right)\right)^2 + \frac{1}{2}(\sinh(1) + 1) - 4\cosh\left(\frac{1}{2}\right)\sinh\left(\frac{1}{2}\right)\right]\psi \tag{1b}$$

in which $\bar{E}, \bar{G}, \bar{I}, \bar{A}, w,$ and ψ denote, respectively, the Young's modulus, shear modulus, moment inertia, cross-sectional area, deflection, and angel of rotation for the links of unit cell.

Thereby, for a cantilever beam with constructed load P at the free end, it gives

$$\delta_p = w(\ell) = \frac{P\ell^3}{3\,\bar{E}\bar{I}} + \frac{6}{5}\frac{P\ell}{\bar{G}\bar{A}}\left(1 + \frac{\cosh(\vartheta\ell) - \sinh(\vartheta\ell) - 1}{\vartheta\ell}\right), \tag{2a}$$

$$\theta = \phi(\ell) = \frac{P\ell^2}{2\,\bar{E}\bar{I}} + \frac{6}{5}\frac{P}{\bar{G}\bar{A}}[1 + \sinh(\vartheta\ell) - \cosh(\vartheta\ell)] \tag{2b}$$

in which

$$\vartheta = \sqrt{\frac{\frac{\overline{GA}}{\overline{EI}}\frac{\alpha_3}{\alpha_1}}{\frac{\alpha_2}{\alpha_1} - \alpha_1}} \tag{3}$$

$$\alpha_1 = cosh\left(\frac{1}{2}\right) - 12\left[cosh\left(\frac{1}{2}\right) - 2sinh\left(\frac{1}{2}\right)\right]$$

$$\alpha_2 = \left(cosh\left(\frac{1}{2}\right)\right)^2 + 6[sinh(1) - 1] - 24cosh\left(\frac{1}{2}\right)\left[cosh\left(\frac{1}{2}\right) - 2sinh\left(\frac{1}{2}\right)\right]$$

$$\alpha_3 = \left(cosh\left(\frac{1}{2}\right)\right)^2 + \frac{1}{2}[sinh(1) + 1] - 4cosh\left(\frac{1}{2}\right)sinh\left(\frac{1}{2}\right)$$

To capture the equivalent bending moment at the free end of the strut causing the same rotation, one will have

$$\frac{P\ell^2}{2\,\overline{EI}} + \frac{6}{5}\frac{P}{\overline{GA}}(1 + \sinh(\vartheta\ell) - \cosh(\vartheta\ell)) = \frac{M\ell}{\overline{EI}} \rightarrow M = \frac{P\ell}{2} + \frac{6}{5}\frac{P}{\ell}\frac{\overline{EI}}{\overline{GA}}[1 + \sinh(\vartheta\ell) - \cosh(\vartheta\ell)]. \tag{4}$$

Therefore, the lateral deflection caused by applying the both concentrated load P and bending moment M at the free end can be written as follows:

$$\delta = \delta_P + \delta_M = \frac{P\ell^3}{3\,\overline{EI}} + \frac{6}{5}\frac{P\ell}{\overline{GA}}\left(1 + \frac{\cosh(\vartheta\ell) - \sinh(\vartheta\ell) - 1}{\vartheta\ell}\right) - \left[\frac{P\ell}{2} + \frac{6}{5}\frac{P}{\ell}\frac{\overline{EI}}{\overline{GA}}(1 + \sinh(\vartheta\ell) - \cosh(\vartheta\ell))\right]\frac{\ell^2}{2\,\overline{EI}} = \frac{P\ell^3}{12\,\overline{EI}} + \frac{3}{5}\frac{P\ell}{\overline{GA}} + \frac{6}{5}\frac{P\ell}{\overline{GA}}\left(\frac{\left(1 + \frac{\vartheta\ell}{2}\right)\cosh(\vartheta\ell) - \left(1 + \frac{\vartheta\ell}{2}\right)\sinh(\vartheta\ell) - 1}{\vartheta\ell}\right). \tag{5}$$

As a result, it yields

$$P = \frac{\delta}{\frac{\ell^3}{12\overline{EI}} + \frac{3\ell}{5\overline{GA}} + \frac{6}{5\overline{GA}}\left(\frac{\left(1+\frac{\vartheta\ell}{2}\right)\cosh(\vartheta\ell) - \left(1+\frac{\vartheta\ell}{2}\right)\sinh(\vartheta\ell) - 1}{\vartheta}\right)}. \tag{6}$$

It should be noticed that, due to the in-plane deformation, the link $c_1a_1b_1d_1a_2c_2$ has 18° of freedom. However, by considering the following reasonable assumptions considered by Hedayati et al. [69], the number of degrees of freedom can be reduced to 6 as depicted in Fig. 3:

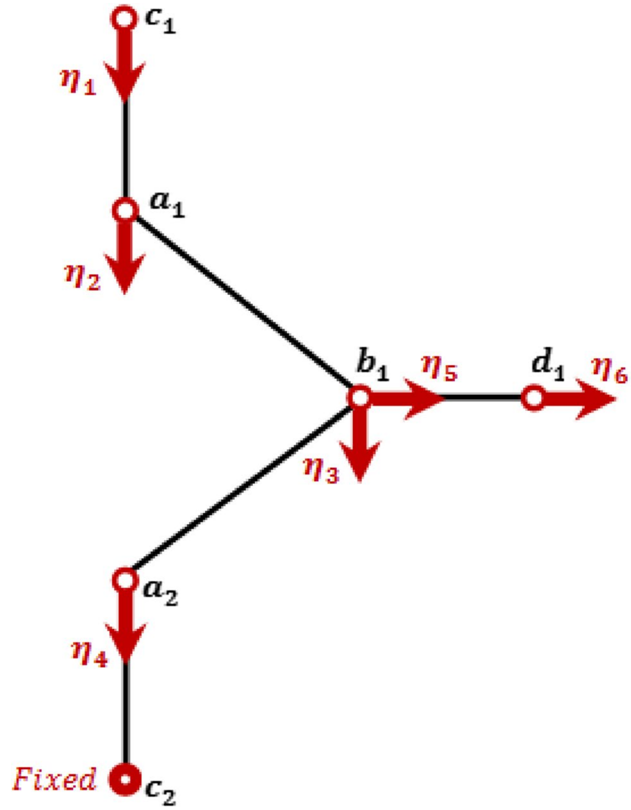

Fig. 3 Degrees of freedom for the link $c_1a_1b_1d_1a_2c_2$ of the unit cell

- The vertices of link do not enable to rotate.
- The points a_1, a_2, c_1 enable only to displace vertically.
- The points b_1 and d_1 displace the same vertically, but different horizontally.
- The point c_2 is fixed.

Thereafter, the degrees of freedom $\eta_i (i = 1,2, \ldots, 6)$ can be related to the associated external force $\Gamma_i (i = 1,2, \ldots, 6)$ in the following form:

$$\begin{Bmatrix} \Gamma_1 \\ \Gamma_2 \\ \Gamma_3 \\ \Gamma_4 \\ \Gamma_5 \\ \Gamma_6 \end{Bmatrix} = \begin{bmatrix} S_{11} & S_{12} & S_{13} & S_{14} & S_{15} & S_{16} \\ S_{21} & S_{22} & S_{23} & S_{24} & S_{25} & S_{26} \\ S_{31} & S_{32} & S_{33} & S_{34} & S_{35} & S_{36} \\ S_{41} & S_{42} & S_{43} & S_{44} & S_{45} & S_{46} \\ S_{51} & S_{52} & S_{53} & S_{54} & S_{55} & S_{56} \\ S_{61} & S_{62} & S_{63} & S_{64} & S_{65} & S_{66} \end{bmatrix} \begin{Bmatrix} \eta_1 \\ \eta_2 \\ \eta_3 \\ \eta_4 \\ \eta_5 \\ \eta_6 \end{Bmatrix}. \tag{7}$$

To extract the elements of the stiffness matrix column by column, the displacements corresponding to each degree of freedom are achieved separately in such a way that the related degree of freedom is supposed to be unit and the other ones are zero.

2.1 For $\eta_1 = 1$ and $\eta_2 = \eta_3 = \eta_4 = \eta_5 = \eta_6 = 0$

It means that the point c_1 displaces downwards by unity. Consequently, it causes the following associated forces in the struts:

$$\Gamma_1 = \frac{2\overline{\overline{AE}}}{\ell}, \Gamma_2 = -\frac{2\overline{\overline{AE}}}{\ell}, \Gamma_3 = \Gamma_4 = \Gamma_5 = \Gamma_6 = 0. \tag{8}$$

2.2 For $\eta_2 = 1$ and $\eta_1 = \eta_3 = \eta_4 = \eta_5 = \eta_6 = 0$

It means that the point a_1 (the vertices of links $a_1b_1, a_1b_2, a_1b_3, a_1b_4$) displaces downwards by unity. As a result, it leads to the following associated forces in the struts:

$$\Gamma_1 = -\frac{2\overline{\overline{AE}}}{\ell}, \Gamma_4 = \Gamma_6 = 0$$

$$\Gamma_2 = \frac{2\overline{\overline{AE}}}{\ell} + 4 \times \left(\frac{1}{\frac{\ell^3}{6\overline{\overline{EI}}} + \frac{6\ell}{5\overline{\overline{GA}}} + \frac{12}{5\overline{\overline{GA}}}\left(\frac{\left(1+\frac{\vartheta\ell}{2}\right)cosh(\vartheta\ell) - \left(1+\frac{\vartheta\ell}{2}\right)sinh(\vartheta\ell) - 1}{\vartheta} \right)} + \frac{\overline{\overline{AE}}}{2\ell} \right)$$

$$\Gamma_3 = -4 \times \left(\frac{1}{\frac{\ell^3}{6\overline{\overline{EI}}} + \frac{6\ell}{5\overline{\overline{GA}}} + \frac{12}{5\overline{\overline{GA}}}\left(\frac{\left(1+\frac{\vartheta\ell}{2}\right)\cosh(\vartheta\ell) - \left(1+\frac{\vartheta\ell}{2}\right)\sinh(\vartheta\ell) - 1}{\vartheta} \right)} + \frac{\overline{\overline{AE}}}{2\ell} \right) \tag{9}$$

$$\Gamma_5 = 4 \times \left(\frac{1}{\frac{\ell^3}{6\overline{\overline{EI}}} + \frac{6\ell}{5\overline{\overline{GA}}} + \frac{12}{5\overline{\overline{GA}}}\left(\frac{\left(1+\frac{\vartheta\ell}{2}\right)cosh(\vartheta\ell) - \left(1+\frac{\vartheta\ell}{2}\right)sinh(\vartheta\ell) - 1}{\vartheta} \right)} - \frac{\overline{\overline{AE}}}{2\ell} \right).$$

2.3 For $\eta_3 = 1$ and $\eta_1 = \eta_2 = \eta_4 = \eta_5 = \eta_6 = 0$

It means that the point b_1 (similarly, the points b_2, b_3, b_4) displaces downwards by unity. Therefore, the correspondence forces in the struts become the following:

$$\Gamma_1 = \Gamma_5 = \Gamma_6 = 0$$

$$\Gamma_2 = \Gamma_4 = -4 \times \left(\frac{1}{\frac{\ell^3}{6\overline{\overline{EI}}} + \frac{6\ell}{5\overline{\overline{GA}}} + \frac{12}{5\overline{\overline{GA}}}\left(\frac{\left(1+\frac{\vartheta\ell}{2}\right)\cosh(\vartheta\ell) - \left(1+\frac{\vartheta\ell}{2}\right)\sinh(\vartheta\ell) - 1}{\vartheta} \right)} - \frac{\overline{\overline{AE}}}{2\ell} \right) \tag{10}$$

$$\Gamma_3 = 4 \times \left(\frac{1}{\frac{\ell^3}{12\overline{\overline{EI}}} + \frac{3\ell}{5\overline{\overline{GA}}} + \frac{6}{5\overline{\overline{GA}}}\left(\frac{\left(1+\frac{\vartheta\ell}{2}\right)cosh(\vartheta\ell) - \left(1+\frac{\vartheta\ell}{2}\right)sinh(\vartheta\ell) - 1}{\vartheta} \right)} + \frac{\overline{\overline{AE}}}{\ell} \right).$$

2.4 For $\eta_4 = 1$ and $\eta_1 = \eta_2 = \eta_3 = \eta_5 = \eta_6 = 0$

It means that the point a_2 (the vertices of links $a_2b_1, a_2b_2, a_2b_3, a_2b_4$) displaces downwards by unity. Consequently, the associated forces in the struts can be written as follows:

$$\Gamma_1 = \Gamma_2 = \Gamma_6 = 0$$

$$\Gamma_3 = -4 \times \left(\frac{1}{\frac{\ell^3}{6\overline{\overline{EI}}} + \frac{6\ell}{5\overline{\overline{GA}}} + \frac{12}{5\overline{\overline{GA}}}\left(\frac{\left(1+\frac{\vartheta\ell}{2}\right)\cosh(\vartheta\ell) - \left(1+\frac{\vartheta\ell}{2}\right)\sinh(\vartheta\ell) - 1}{\vartheta} \right)} + \frac{\overline{\overline{AE}}}{2\ell} \right) \tag{11}$$

$$\Gamma_4 = \frac{2\overline{\overline{AE}}}{\ell} + 4 \times \left(\frac{1}{\frac{\ell^3}{6\overline{\overline{EI}}} + \frac{6\ell}{5\overline{\overline{GA}}} + \frac{12}{5\overline{\overline{GA}}}\left(\frac{\left(1+\frac{\vartheta\ell}{2}\right)cosh(\vartheta\ell) - \left(1+\frac{\vartheta\ell}{2}\right)sinh(\vartheta\ell) - 1}{\vartheta} \right)} + \frac{\overline{\overline{AE}}}{2\ell} \right)$$

$$\Gamma_5 = -4 \times \left(\frac{1}{\frac{\ell^3}{6\overline{\overline{EI}}} + \frac{6\ell}{5\overline{\overline{GA}}} + \frac{12}{5\overline{\overline{GA}}}\left(\frac{\left(1+\frac{\vartheta\ell}{2}\right)cosh(\vartheta\ell) - \left(1+\frac{\vartheta\ell}{2}\right)sinh(\vartheta\ell) - 1}{\vartheta} \right)} - \frac{\overline{\overline{AE}}}{2\ell} \right).$$

2.5 For $\eta_5 = 1$ and $\eta_1 = \eta_2 = \eta_3 = \eta_4 = \eta_6 = 0$

It means that the point b_1 (similarly, the points b_2, b_3, b_4) displaces horizontally by unity. As a result, the associated forces in the struts are derived as follows:

$$\Gamma_1 = \Gamma_3 = 0$$

$$\Gamma_2 = 4 \times \left(\frac{1}{\frac{\ell^3}{6\overline{\overline{EI}}} + \frac{6\ell}{5\overline{\overline{GA}}} + \frac{12}{5\overline{\overline{GA}}}\left(\frac{\left(1+\frac{\vartheta\ell}{2}\right)cosh(\vartheta\ell) - \left(1+\frac{\vartheta\ell}{2}\right)sinh(\vartheta\ell) - 1}{\vartheta} \right)} - \frac{\overline{\overline{AE}}}{2\ell} \right)$$

$$\Gamma_4 = -4 \times \left(\frac{1}{\frac{\ell^3}{6\overline{\overline{EI}}} + \frac{6\ell}{5\overline{\overline{GA}}} + \frac{12}{5\overline{\overline{GA}}}\left(\frac{\left(1+\frac{\vartheta\ell}{2}\right)\cosh(\vartheta\ell) - \left(1+\frac{\vartheta\ell}{2}\right)\sinh(\vartheta\ell) - 1}{\vartheta} \right)} - \frac{\overline{\overline{AE}}}{2\ell} \right) \tag{12}$$

$$\Gamma_5 = 4 \times \left(\frac{1}{\frac{\ell^3}{12\bar{E}\bar{I}} + \frac{3\ell}{5\bar{G}\bar{A}} + \frac{6}{5\bar{G}\bar{A}}\left(\frac{\left(1+\frac{\vartheta\ell}{2}\right)cosh(\vartheta\ell) - \left(1+\frac{\vartheta\ell}{2}\right)sinh(\vartheta\ell) - 1}{\vartheta} \right)} + \frac{5\bar{A}\bar{E}}{\ell} \right)$$

$$\Gamma_6 = -4 \times \left(\frac{2\bar{A}\bar{E}}{\ell} \right).$$

2.6 For $\eta_6 = 1$ and $\eta_1 = \eta_2 = \eta_3 = \eta_4 = \eta_5 = 0$

It means that the point d_1 (similarly, the points d_2, d_3, d_4) displaces horizontally by unity. Thereby, the correspondence forces in the struts can be expressed as follows:

$$\Gamma_1 = \Gamma_2 = \Gamma_3 = \Gamma_4 = 0$$

$$\Gamma_5 = -4\left(\frac{2\bar{A}\bar{E}}{\ell} \right) \tag{13}$$

$$\Gamma_6 = 4\left(\frac{2\bar{A}\bar{E}}{\ell} \right).$$

Thereafter, the elements of the stiffness matrix can be achieved as presented in Appendix.

Similar to the assumption considered by Hedayati et al. [69], it is supposed that the external force acts vertically on point c_1 of the refined truncated cube lattice structure, which results in an additional horizontal force equal to $\frac{8\bar{A}\bar{E}(\eta_6-\eta_5)}{\ell}$ at point d_1. As a result, one will have the following:

$$\begin{Bmatrix} P \\ 0 \\ 0 \\ 0 \\ 0 \\ 0 \end{Bmatrix} = \begin{bmatrix} S_{11} & S_{12} & 0 & 0 & 0 & 0 \\ S_{21} & S_{22} & S_{23} & 0 & S_{25} & 0 \\ 0 & S_{32} & S_{33} & S_{34} & 0 & 0 \\ 0 & 0 & S_{43} & S_{44} & S_{45} & 0 \\ 0 & S_{52} & 0 & S_{54} & S_{55} & S_{56} \\ 0 & 0 & 0 & 0 & 2S_{65} & 2S_{66} \end{bmatrix} \begin{Bmatrix} \eta_1 \\ \eta_2 \\ \eta_3 \\ \eta_4 \\ \eta_5 \\ \eta_6 \end{Bmatrix}. \tag{14}$$

The elastic modulus of the refined truncated cube unit cell can be calculated as follows:

$$E = \frac{F_u L_u}{A_u \delta_u} = \frac{P}{\left(1+\sqrt{2}\right)\ell\eta_1}, \tag{15}$$

where F_u, L_u, A_u, and δ_u represent, respectively, the applied load, length, cross-sectional area, and shortening of the unit cell.

Through inversion of the above equation, η_1 can be extracted as a function of P. Therefore, it yields the following:

$$\begin{aligned} E = \big(&S_{11}S_{22}S_{33}S_{66}S_{45}S_{54} - S_{11}S_{22}S_{33}S_{44}S_{55}S_{66} \\ &+S_{11}S_{22}S_{55}S_{66}S_{34}S_{43} + S_{11}S_{33}S_{44}S_{66}S_{25}S_{52} \\ &-S_{11}S_{66}S_{25}S_{52}S_{34}S_{43} + 2S_{11}S_{66}S_{34}S_{45}S_{23}S_{25} \\ &+S_{11}S_{44}S_{55}S_{66}S_{23}S_{32} - S_{11}S_{66}S_{45}S_{54}S_{23}S_{32} \\ &+S_{33}S_{44}S_{55}S_{66}S_{12}S_{21} - S_{33}S_{66}S_{45}S_{54}S_{12}S_{21} \\ &-S_{55}S_{66}S_{12}S_{21}S_{34}S_{43} + S_{11}S_{22}S_{33}S_{44}S_{56}S_{65} \\ &-S_{33}S_{44}S_{12}S_{21}S_{56}S_{65} - S_{11}S_{44}S_{23}S_{32}S_{56}S_{65} \\ &-S_{11}S_{22}S_{34}S_{43}S_{56}S_{65} + S_{12}S_{21}S_{34}S_{43}S_{56}S_{65}\big)/ \\ &\big[\big(S_{66}S_{22}S_{33}S_{45}S_{54} - S_{66}S_{22}S_{33}S_{55}S_{44} \\ &+S_{22}S_{55}S_{66}S_{34}S_{43} + S_{33}S_{44}S_{66}S_{25}S_{52} \\ &-S_{66}S_{25}S_{52}S_{34}S_{43} + 2S_{66}S_{45}S_{34}S_{23}S_{25} \\ &+S_{44}S_{55}S_{66}S_{23}S_{32} - S_{66}S_{45}S_{54}S_{23}S_{32} \\ &+S_{22}S_{33}S_{44}S_{56}S_{65} - S_{44}S_{23}S_{32}S_{56}S_{65} \\ &-S_{22}S_{34}S_{43}S_{56}S_{65}\big)\left(1+\sqrt{2}\right)\ell\big] \end{aligned} \tag{16}$$

Moreover, to obtain the Poisson's ratio, it can be introduced as the ratio of horizontal to vertical displacements in the following form

$$\nu = \frac{2\eta_6}{\eta_1}. \tag{17}$$

Consequently, one will have the following:

$$\begin{aligned} \nu = 2S_{12}S_{56}&\left(S_{33}S_{44}S_{25} - S_{25}S_{34}S_{43} + S_{23}S_{34}S_{45}\right)/ \\ \big(&S_{22}S_{33}S_{66}S_{45}S_{54} - S_{22}S_{33}S_{44}S_{55}S_{66} \\ &+S_{22}S_{55}S_{66}S_{34}S_{43} + S_{33}S_{44}S_{66}S_{25}S_{52} \\ &-S_{66}S_{25}S_{52}S_{34}S_{43} + 2S_{66}S_{23}S_{25}S_{34}S_{45} \\ &+S_{44}S_{55}S_{66}S_{23}S_{32} - S_{66}S_{23}S_{32}S_{45}S_{54} \\ &+S_{22}S_{33}S_{44}S_{56}S_{65} - S_{44}S_{23}S_{32}S_{56}S_{65} \\ &+S_{22}S_{34}S_{43}S_{56}S_{65}\big). \end{aligned} \tag{18}$$

3 Nonlocal strain gradient beam model for porous micro/nano-beams

Within the framework of the refined hyperbolic shear deformation beam theory, the components of displacement field along different coordinate directions can be given as follows:

$$\begin{aligned} u_x(x,z,t) &= u(x,t) - z\frac{\partial w(x,t)}{\partial x} + \left[zcosh\left(\frac{1}{2}\right) - hsinh\left(\frac{z}{h}\right) \right]\psi(x,t) \\ u_y(x,z,t) &= 0 \\ u_z(x,z,t) &= w(x,t), \end{aligned} \tag{19}$$

in which $u$and w stand for the displacement components of the micro/nano-beam along x- and z-axes, respectively. Moreover, ψ denotes the rotation relevant to the cross section of nano-beam at neutral plane normal about y-axis.

Thereafter, the non-zero strain components can be governed as follows:

$$\epsilon_{xx} = \epsilon^0_{xx} + z\kappa^{(1)}_{xx} + \left[z\cosh\left(\frac{1}{2}\right) - h\sinh\left(\frac{z}{h}\right)\right]\kappa^{(2)}_{xx} = \frac{\partial u}{\partial x} + \frac{1}{2}\left(\frac{\partial w}{\partial x}\right)^2 - z\frac{\partial^2 w}{\partial x^2} + \left[z\cosh\left(\frac{1}{2}\right) - h\sinh\left(\frac{z}{h}\right)\right]\frac{\partial \psi}{\partial x} \tag{20a}$$

$$\gamma_{xz} = \left[\cosh\left(\frac{1}{2}\right) - \cosh\left(\frac{z}{h}\right)\right]\psi, \tag{20b}$$

in which ϵ^0_{xx} denote the mid-plane strain components, $\kappa^{(1)}_{xx}$ is the first-order curvature component, and $\kappa^{(2)}_{xx}$ is the higher order curvature component.

As it has been reported in the specialized literature on the subject of size dependence, it has been indicated that small-scale effects may cause two entirely different influences incorporating hardening-stiffness or stiffening-stiffness features. Motivated by this fact, Lim et al. [43] proposed a new unconventional continuum theory namely as nonlocal strain gradient elasticity theory which contains the both nonlocal and strain gradient size effects simultaneously. As a result, the total nonlocal strain gradient stress tensor Λ for a beam-type structure can be expressed as follows [43]:

$$\Lambda_{xx} = \sigma_{xx} - \frac{\partial \sigma^*_{xx}}{\partial x} \tag{21a}$$

$$\Lambda_{xz} = \sigma_{xz} - \frac{\partial \sigma^*_{xz}}{\partial x}, \tag{21b}$$

where σ and σ^* are the stress and higher order stress tensors, respectively, which can be defined as follows:

$$\sigma_{ij} = \int_\Omega \left\{\varrho_1\left(|\mathcal{X}' - \mathcal{X}|\right)C_{ijkl}\epsilon_{kl}\left(\mathcal{X}'\right)\right\}d\Omega \tag{22a}$$

$$\sigma^*_{ij} = l^2\int_\Omega \left\{\varrho_2\left(|\mathcal{X}' - \mathcal{X}|\right)C_{ijkl}\frac{\partial \epsilon_{kl}\left(\mathcal{X}'\right)}{\partial x}\right\}d\Omega, \tag{22b}$$

in which C is the stiffness matrix, $\varrho_1$and ϱ_2 are, respectively, the principal attenuation kernel function including the nonlocality and the additional kernel function associated with the nonlocality effect of the first-order strain gradient field, $\mathcal{X}$ and $\mathcal{X}$' in order represent a point and any point else in the body, and l stands for the internal strain gradient length scale parameter. Following the method of Eringen, the constitutive relationship corresponding to the total nonlocal strain gradient stress tensor of a beam-type structure can be obtained as follows:

$$\left(1 - \mu^2\frac{\partial^2}{\partial x^2}\right)\Lambda_{ij} = C_{ijkl}\epsilon_{kl} - l^2 C_{ijkl}\frac{\partial^2 \epsilon_{kl}}{\partial x^2}, \tag{23}$$

where μ is the nonlocal parameter. As a result, the nonlocal strain gradient constitutive relations for a hyperbolic shear deformable micro/nano-beam made of nanoporous material can be written as follows:

$$\left(1 - \mu^2\frac{\partial^2}{\partial x^2}\right)\left\{\begin{array}{c}\sigma_{xx}\\ \sigma_{xz}\end{array}\right\} = \left(1 - l^2\frac{\partial^2}{\partial x^2}\right)\left[\begin{array}{cc}Q_{11} & 0\\ 0 & Q_{44}\end{array}\right]\left\{\begin{array}{c}\epsilon_{xx}\\ \gamma_{xz}\end{array}\right\}, \tag{24}$$

in which

$$Q_{11} = \frac{E}{1-\nu^2}, Q_{44} = \frac{E}{2(1+\nu)}. \tag{25}$$

Therefore, based upon the nonlocal strain gradient hyperbolic shear deformable beam model, the total strain energy of a micro/nano-beam can be expressed as follows:

$$\Pi_s = \frac{1}{2}\int_0^L\int_S\left(\sigma_{ij}\epsilon_{ij} + \sigma^*_{ij}\nabla\epsilon_{ij}\right)dSdx = \frac{1}{2}\int_0^L\left\{N_{xx}\epsilon^0_{xx} + M_{xx}\kappa^{(1)}_{xx} + R_{xx}\kappa^{(2)}_{xx} + Q_x\gamma_{xz}\right\}dx, \tag{26}$$

where S is the cross-sectional area of the micro/nano-beam, and the stress resultants are in the following forms:

$$N_{xx} - \mu^2\frac{\partial^2 N_{xx}}{\partial x^2} = A^*_{11}\left(\epsilon^0_{xx} - l^2\frac{\partial^2\epsilon^0_{xx}}{\partial x^2}\right)$$

$$M_{xx} - \mu^2\frac{\partial^2 M_{xx}}{\partial x^2} = D^*_{11}\left(\kappa^{(1)}_{xx} - l^2\frac{\partial^2\kappa^{(1)}_{xx}}{\partial x^2}\right) + F^*_{11}\left(\kappa^{(2)}_{xx} - l^2\frac{\partial^2\kappa^{(2)}_{xx}}{\partial x^2}\right)$$

$$R_{xx} - \mu^2\frac{\partial^2 R_{xx}}{\partial x^2} = F^*_{11}\left(\kappa^{(1)}_{xx} - l^2\frac{\partial^2\kappa^{(1)}_{xx}}{\partial x^2}\right) + H^*_{11}\left(\kappa^{(2)}_{xx} - l^2\frac{\partial^2\kappa^{(2)}_{xx}}{\partial x^2}\right), \tag{27}$$

$$Q_x - \mu^2\frac{\partial^2 Q_x}{\partial x^2} = A^*_{44}\left(\gamma_{xz} - l^2\frac{\partial^2\gamma_{xz}}{\partial x^2}\right)$$

in which

$$\{N_{xx}, M_{xx}, R_{xx}\} = b\int_{-\frac{h}{2}}^{\frac{h}{2}}\Lambda^{(k)}_{xx}\left\{1, z, zcosh\left(\frac{1}{2}\right) - hsinh\left(\frac{z}{h}\right)\right\}dz$$

$$Q_x = b\int_{-\frac{h}{2}}^{\frac{h}{2}}\Lambda^{(k)}_{xz}\left\{\cosh\left(\frac{1}{2}\right) - \cosh\left(\frac{z}{h}\right)\right\}dz \tag{28}$$

and

$$\{A_{11}^*, D_{11}^*, F_{11}^*, H_{11}^*\} = bQ_{11}\int_{-\frac{h}{2}}^{\frac{h}{2}} \left\{1, z^2, z^2 cosh\left(\frac{1}{2}\right) - zhsinh\left(\frac{z}{h}\right), \left(zcosh\left(\frac{1}{2}\right) - hsinh\left(\frac{z}{h}\right)\right)^2\right\} dz$$

$$\{A_{44}^*\} = bQ_{44}\int_{-\frac{h}{2}}^{\frac{h}{2}} \left\{\cosh\left(\frac{1}{2}\right) - \cosh\left(\frac{z}{h}\right)\right\} dz. \tag{29}$$

Furthermore, the kinetic energy of a micro/nano-beam modeled via the nonlocal strain gradient hyperbolic shear deformable beam model can be presented as follows:

$$\begin{aligned} \Pi_T &= \frac{1}{2}\int_0^L \int_S \rho \left\{ \left(\frac{\partial u_x}{\partial t}\right)^2 + \left(\frac{\partial u_z}{\partial t}\right)^2 \right\} dS dx \\ &= \frac{1}{2}\int_0^L \left\{ I_0\left(\frac{\partial u}{\partial t}\right)^2 + I_2\left(\frac{\partial^2 w}{\partial x \partial t}\right)^2 + I_3 \frac{\partial^2 w}{\partial x \partial t}\frac{\partial \psi}{\partial t} \right. \\ &\quad \left. + I_4\left(\frac{\partial \psi}{\partial t}\right)^2 + I_0\left(\frac{\partial w}{\partial x}\right)^2 \right\} dx, \end{aligned} \tag{30}$$

where

$$\{I_0, I_2, I_3, I_4\} = b\rho\int_{-\frac{h}{2}}^{\frac{h}{2}} \left\{1, z^2, z^2\cosh\left(\frac{1}{2}\right) - zh\sinh\left(\frac{z}{h}\right), \left(z\cosh\left(\frac{1}{2}\right) - h\sinh\left(\frac{z}{h}\right)\right)^2\right\} dz. \tag{31}$$

In addition, the work done by the transverse force q can be introduced as follows:

$$\Pi_w = \int_0^L q(x,t) w dx. \tag{32}$$

Thereby, using the Hamilton's principle, the governing differential equations in terms of stress resultants can be constructed as follows:

$$\frac{\partial N_{xx}}{\partial x} = I_0 \frac{\partial^2 u}{\partial t^2} \tag{33a}$$

$$\frac{\partial^2 M_{xx}}{\partial x^2} + \frac{\partial N_{xx}}{\partial x}\frac{\partial w}{\partial x} + \frac{\partial}{\partial x}\left(N_{xx}\frac{\partial w}{\partial x}\right) + q = I_0\frac{\partial^2 w}{\partial t^2} - I_2\frac{\partial^4 w}{\partial x^2 \partial t^2} - I_3\frac{\partial^3 \psi}{\partial x \partial t^2} \tag{33b}$$

$$\frac{\partial R_{xx}}{\partial x} - Q_x = I_3\frac{\partial^3 w}{\partial x \partial t^2} + I_4\frac{\partial^2 \psi}{\partial t^2}. \tag{33c}$$

Afterwards, by substituting Eq. (33a) in equations (33b) and (33c), and using Eq. (29), the nonlocal strain gradient governing differential equations for a hyperbolic shear deformable micro/nano-beam with immovable end supports can be constructed as follows:

$$\begin{aligned} &\left(1 - l^2\frac{\partial^2}{\partial x^2}\right)\left(D_{11}^*\frac{\partial^4 w}{\partial x^4} - F_{11}^*\frac{\partial^3 \psi}{\partial x^3}\right) \\ &= \left(1 - \mu^2\frac{\partial^2}{\partial x^2}\right)\left(+ N_{xx}\frac{\partial^2 w}{\partial x^2} - I_0\frac{\partial^2 w}{\partial t^2} \right. \\ &\quad \left. + (I_2 - I_3)\frac{\partial^4 w}{\partial x^2 \partial t^2} + (I_3 - I_4)\frac{\partial^3 \psi}{\partial x \partial t^2}\right) \end{aligned} \tag{34a}$$

$$F_{11}^*\frac{\partial^3 w}{\partial x^3} - H_{11}^*\frac{\partial^2 \psi}{\partial x^2} + A_{44}^*\psi = I_4\frac{\partial^3 w}{\partial x \partial t^2} + I_3\frac{\partial^2 \psi}{\partial t^2} \tag{34b}$$

$$N_{xx} = \frac{1}{L}\int_0^L \left\{\frac{A_{11}^*}{2}\left(\frac{\partial w}{\partial x}\right)^2\right\} dx. \tag{34c}$$

4 Analytical solving process for asymptotic solutions

First of all, for extracting the asymptotic solutions associated with the present size-dependent problem, the following dimensionless parameters are introduced:

$$X = \frac{\pi x}{L}, W = \frac{w}{L}, \Psi = \frac{\psi}{\pi}, \tau = \frac{\pi t}{L}\sqrt{\frac{A_{00}}{I_{00}}}, \mathcal{P}_q = \frac{L^3}{\pi^4 A_{00} h^2}$$

$$\{a_{11}^*, a_{44}^*, d_{11}^*, f_{11}^*, h_{11}^*\} = \left\{\frac{L^2 A_{11}^*}{\pi^2 A_{00} h^2}, \frac{A_{44}^*}{A_{00}}, \frac{D_{11}^*}{\pi^2 A_{00} h^2}, \frac{F_{11}^*}{\pi^2 A_{00} h^2}, \frac{H_{11}^*}{\pi^2 A_{00} h^2}\right\} \tag{35}$$

$$\{\bar{I}_0, \bar{I}_2, \bar{I}_3, \bar{I}_4\} = \left\{\frac{L^2 I_0}{\pi^2 I_{00} h^2}, \frac{I_2}{I_{00} h^2}, \frac{I_3}{I_{00} h^2}, \frac{I_4}{I_{00} h^2}\right\},$$

where $A_{00} = Ebh$ and $I_{00} = \rho bh$. Thus, the nonlocal strain gradient governing differential equations of motion for the refined hyperbolic shear deformable micro/nano-beam can be rewritten in the following dimensionless form:

$$\begin{aligned} &\left(1 - \pi^2\mathcal{G}_2^2\frac{\partial^2}{\partial X^2}\right)\left(d_{11}^*\frac{\partial^4 W}{\partial X^4} - f_{11}^*\frac{\partial^3 \Psi}{\partial X^3}\right) = \left(1 - \pi^2\mathcal{G}_1^2\frac{\partial^2}{\partial X^2}\right) \\ &\left[\mathcal{P}_q - \bar{I}_0\frac{\partial^2 W}{\partial \tau^2} + (\bar{I}_2 - \bar{I}_3)\frac{\partial^4 W}{\partial X^2 \partial \tau^2} + (\bar{I}_3 - \bar{I}_4)\frac{\partial^3 \Psi}{\partial X \partial \tau^2} \right. \\ &\left. + \pi\left(\int_0^\pi \left\{\frac{a_{11}^*}{2}\left(\frac{\partial W}{\partial X}\right)^2\right\} dX\right)\frac{\partial^2 W}{\partial X^2}\right] \end{aligned} \tag{36a}$$

$$f_{11}^*\frac{\partial^3 W}{\partial X^3} - h_{11}^*\frac{\partial^2 \Psi}{\partial X^2} - a_{44}^*\Psi = \bar{I}_4\frac{\partial^3 W}{\partial X \partial \tau^2} + \bar{I}_3\frac{\partial^2 \Psi}{\partial \tau^2}. \tag{36b}$$

Now, an improved perturbation method namely as two-stepped perturbation technique [70–82] is put to use. To continue the solving process, the independent variables are defined as the summations of the solutions corresponding to different orders of the first perturbation parameter, ϵ, as follows:

$$\bar{W}\left(X,\hat{\tau},\epsilon\right)=\sum_{i=1}\epsilon^i\bar{W}_i(X,\hat{\tau}),\bar{\Psi}\left(X,\hat{\tau},\epsilon\right)=\sum_{i=1}\epsilon^i\bar{\Psi}_i\left(X,\hat{\tau}\right), \tag{37}$$

in which $\hat{\tau}=\epsilon\tau$ is considered to improve the efficiency of the perturbation approach for capturing the solution of vibration problem. In such a case, the nonlocal strain gradient governing differential equations of motion take the following form:

$$\begin{aligned}&\left(1-\pi^2\mathcal{G}_2^2\frac{\partial^2}{\partial X^2}\right)\left(d_{11}^*\frac{\partial^4\bar{W}}{\partial X^4}-f_{11}^*\frac{\partial^3\bar{\Psi}}{\partial X^3}\right)=\left(1-\pi^2\mathcal{G}_1^2\frac{\partial^2}{\partial X^2}\right)\\&\left[\mathcal{P}_q-\epsilon^2\left(\bar{I}_0\frac{\partial^2\bar{W}}{\partial\hat{\tau}^2}+\left(\bar{I}_2-\bar{I}_3\right)\frac{\partial^4\bar{W}}{\partial X^2\partial\hat{\tau}^2}+\left(\bar{I}_3-\bar{I}_4\right)\frac{\partial^3\bar{\Psi}}{\partial X\partial\hat{\tau}^2}\right)\right.\\&\left.+\pi\left(\int_0^\pi\left\{\frac{a_{11}^*}{2}\left(\frac{\partial\bar{W}}{\partial X}\right)^2\right\}dX\right)\frac{\partial^2\bar{W}}{\partial X^2}\right]\end{aligned} \tag{38a}$$

$$f_{11}^*\frac{\partial^3\bar{W}}{\partial X^3}-h_{11}^*\frac{\partial^2\bar{\Psi}}{\partial X^2}-a_{44}^*\bar{\Psi}=\epsilon^2\left(\bar{I}_4\frac{\partial^3\bar{W}}{\partial X\partial\hat{\tau}^2}+\bar{I}_3\frac{\partial^2\bar{\Psi}}{\partial\hat{\tau}^2}\right). \tag{38b}$$

It is assumed that the immovable ends of the micro/nano-beam are simply supported and the initial conditions are as follows:

$$\bar{W}\Big|_{\hat{\tau}=0}=0,\ \frac{\partial\bar{W}}{\partial\hat{\tau}}\Big|_{\hat{\tau}=0}=0,\ \bar{\Psi}\Big|_{\hat{\tau}=0}=0,\ \frac{\partial\bar{\Psi}}{\partial\hat{\tau}}\Big|_{\hat{\tau}=0}=0. \tag{39}$$

We substitute Eq. (37) into Eqs. (38a) and (38b) and then collect the expressions with the same order of ϵ result in a set of perturbation equations. Subsequently, the asymptotic solutions corresponding to each individual variable can be obtained as follows:

$$\bar{W}\left(X,\tau,\epsilon\right)=\epsilon A_{10}^{(1)}(\tau)\sin(mX)+O\left(\epsilon^4\right) \tag{40a}$$

$$\bar{\Psi}\left(X,\tau,\epsilon\right)=\epsilon B_{10}^{(1)}(\tau)\sin(mX)+\epsilon^3B_{10}^{(3)}\cos(mX)+O\left(\epsilon^4\right) \tag{40b}$$

$$\begin{aligned}\mathcal{P}_q(X,\tau,\epsilon)=&\left[\left(\frac{m^4\xi_2}{\xi_1}\left(d_{11}^*+f_{11}^*\frac{f_{11}^*m^2+a_{44}^*}{a_{44}^*-h_{11}^*m^2}\right)\right)\left(\epsilon A_{10}^{(1)}(\tau)\right)\right.\\&+\left(\bar{I}_0+m^2\left(\bar{I}_2-\bar{I}_3+\frac{\left(\bar{I}_3-\bar{I}_4\right)\xi_2}{\xi_1}\frac{f_{11}^*m^2+a_{44}^*}{a_{44}^*-h_{11}^*m^2}\right)\right.\\&\left.\left.-\frac{f_{11}^*m^4\xi_2}{(a_{44}^*-h_{11}^*m^2)\xi_1}\left(\bar{I}_4-\bar{I}_3\frac{f_{11}^*m^2+a_{44}^*}{a_{44}^*-h_{11}^*m^2}\right)\right)\frac{\partial^2\left(\epsilon A_{10}^{(1)}(\tau)\right)}{\partial\tau^2}\right]\\&\times\sin(mX)+\left(\frac{\pi^2m^4a_{11}^*}{4}\right)\left(\epsilon A_{10}^{(1)}(\tau)\right)^3\sin(mX)+O\left(\epsilon^4\right),\end{aligned} \tag{40c}$$

where

$$\xi_1=1+\pi^2m^2\mathcal{G}_1^2,\ \xi_2=1+\pi^2m^2\mathcal{G}_2^2. \tag{41}$$

For a free vibration analysis, one will have $\mathcal{P}_q=0$. As a consequence, after applying the Galerkin method, it yields the following:

$$\begin{aligned}&\left[\frac{m^4\xi_2}{\xi_1}\left(d_{11}^*+f_{11}^*\frac{f_{11}^*m^2+a_{44}^*}{a_{44}^*-h_{11}^*m^2}\right)\right]\left(\epsilon A_{10}^{(1)}(\tau)\right)\\&+\left[\bar{I}_0+m^2\left(\bar{I}_2-\bar{I}_3+\frac{\left(\bar{I}_3-\bar{I}_4\right)\xi_2}{\xi_1}\frac{f_{11}^*m^2+a_{44}^*}{a_{44}^*-h_{11}^*m^2}\right)\right.\\&\left.-\frac{f_{11}^*m^4\xi_2}{(a_{44}^*-h_{11}^*m^2)\xi_1}\left(\bar{I}_4-\bar{I}_3\frac{f_{11}^*m^2+a_{44}^*}{a_{44}^*-h_{11}^*m^2}\right)\right]\frac{\partial^2\left(\epsilon A_{10}^{(1)}(\tau)\right)}{\partial\tau^2}\\&+\left(\frac{\pi^2m^4a_{11}^*}{4}\right)\left(\epsilon A_{10}^{(1)}(\tau)\right)^3=0.\end{aligned} \tag{42}$$

Thereby, the nonlinear nonlocal strain gradient frequency of the micro/nano-beam made of the nanoporous material can be extracted explicitly as follows:

$$\omega_{NL}=\omega_L\sqrt{1+\frac{3\left(\frac{\pi^2m^4a_{11}^*}{4}\right)}{4\left[\frac{m^4\xi_2}{\xi_1}\left(d_{11}^*+f_{11}^*\frac{f_{11}^*m^2+a_{44}^*}{a_{44}^*-h_{11}^*m^2}\right)\right]}W_{max}^2}, \tag{43}$$

where the linear nonlocal strain gradient natural frequency can be defined as follows:

$$\omega_L=\sqrt{\frac{\frac{m^4\xi_2}{\xi_1}\left(d_{11}^*+f_{11}^*\frac{f_{11}^*m^2+a_{44}^*}{a_{44}^*-h_{11}^*m^2}\right)}{\bar{I}_0+m^2\left(\bar{I}_2-\bar{I}_3+\frac{\left(\bar{I}_3-\bar{I}_4\right)\xi_2}{\xi_1}\frac{f_{11}^*m^2+a_{44}^*}{a_{44}^*-h_{11}^*m^2}\right)-\frac{f_{11}^*m^4\xi_2}{(a_{44}^*-h_{11}^*m^2)\xi_1}\left(\bar{I}_4-\bar{I}_3\frac{f_{11}^*m^2+a_{44}^*}{a_{44}^*-h_{11}^*m^2}\right)}} \tag{44}$$

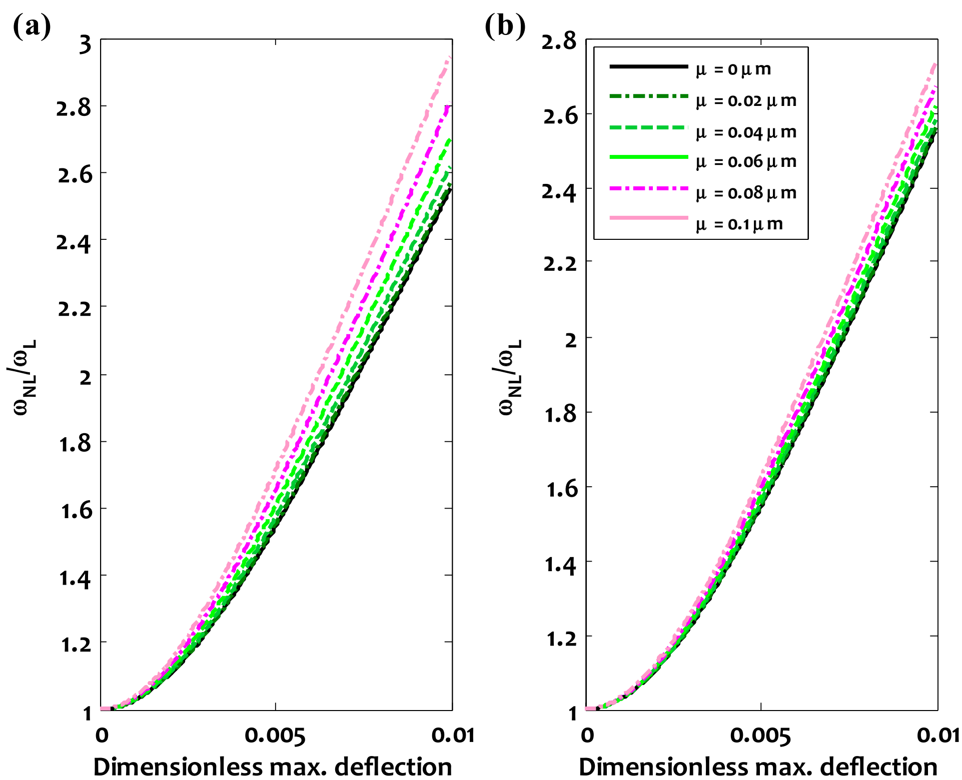

Fig. 4 Variation of frequency ratio with dimensionless maximum deflection of micro/nano-beam made of nanoporous materials corresponding to various nonlocal parameters ($l = 0\,\mu$m, $\ell/r = 10$): **a** $h = 10\,$nm; **b** $h = 15\,$nm

and W_{max} represents the dimensionless maximum deflection of micro/nano-beam made of the nanoporous material.

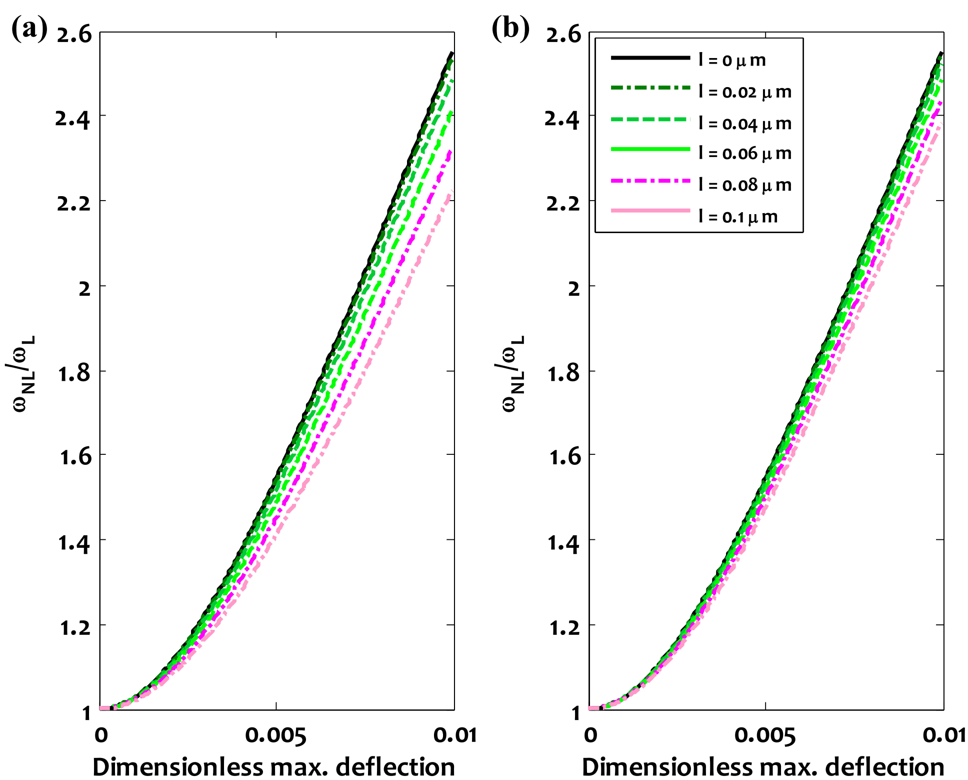

Fig. 5 Variation of frequency ratio with dimensionless maximum deflection of micro/nano-beam made of nanoporous materials corresponding to various strain gradient parameters ($\mu = 0\,\mu$m, $\ell/r = 10$): **a** $h = 10\,$nm; **b** $h = 15\,$nm

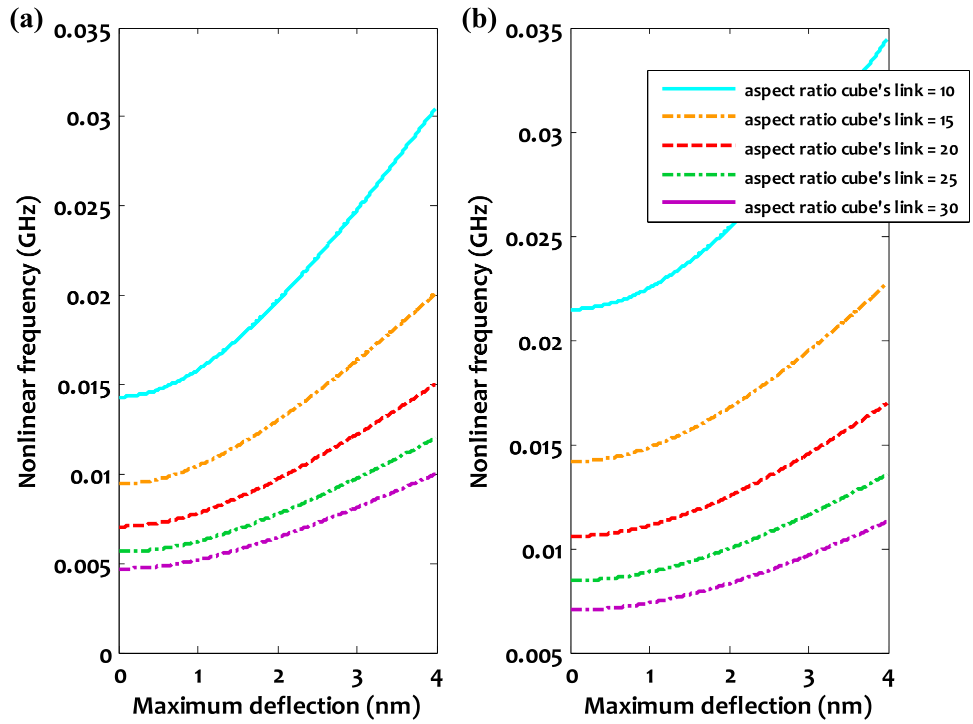

Fig. 6 Nonlinear frequency-deflection response of micro/nano-beams made of nanoporous material with different pore sizes ($\mu = l = 0\,\mu$m): **a** $h = 10\,$nm; **b** $h = 15\,$nm

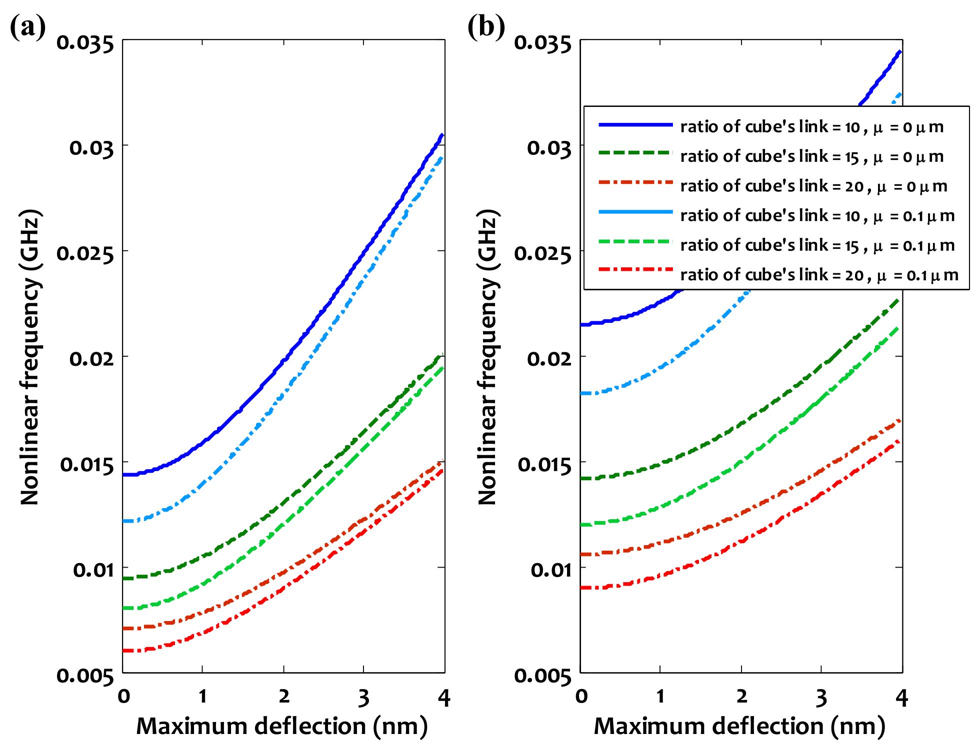

Fig. 7 Size-dependent and size-independent nonlinear frequency-deflection response of micro/nano-beams made of nanoporous material corresponding to different pore sizes ($l = 0\,\mu$m): **a** $h = 10\,$nm; **b** $h = 15\,$nm

5 Results and discussion

Herein, selected numerical results are presented for the size-dependent nonlinear large-amplitude vibrations of micro/nano-beams made of nanoporous material including different pore sizes. It is assumed that the biomaterial is made from Ti6Al4V-ELI Titanium alloy having an elastic modulus of E= 122.3GPa, and Poisson's ratio of ν= 0.342 [83]. In addition, the geometrical parameter of the micro/nano-beam are selected as: $h = b$. In addition, the links of

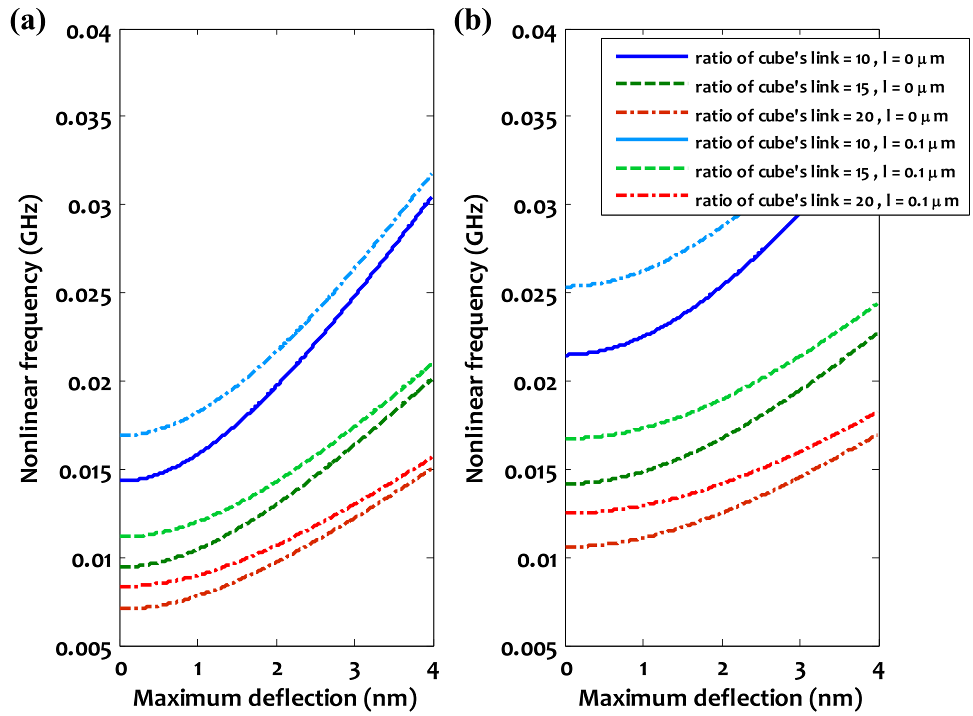

Fig. 8 Size-dependent and size-independent nonlinear frequency-deflection response of micro/nano-beams made of nanoporous material corresponding to different pore sizes ($\mu = 0\,\mu$m): **a** $h = 10\,$nm; **b** $h = 15\,$nm

the refined truncated cubic cells have a circular cross section with radius of r.

In Figs. 4 and 5, the variation of frequency ratio (ω_{NL}/ω_L) with dimensionless maximum deflection of micro/nano-beam is shown corresponding to the different values of nonlocal parameter and strain gradient length-scale parameter, respectively. It is assumed that $L = 500$h and the pore size of $\ell/r = 10$. It can be observed that, by increasing the maximum deflection of micro/nano-beam, both types of size dependence have more significant effect on the frequency ratio, so the gap between different curves increases. This anticipation is more considerable for micro/nano-beams with lower thickness.

Figure 6 displays the nonlinear frequency-deflection response of micro/nano-beams made of nanoporous materials with different pore sizes (various values of ℓ/r). It is supposed that $L = 500$nm. It is seen that, by increasing the pore size, the nonlinear frequency of large-amplitude vibration of micro/nano-beams made of nanoporous material reduces, but the rate of this reduction becomes lower for higher pore size. In addition, the slope of the nonlinear frequency-deflection variation is higher for micro/nano-beams made of nanoporous material with smaller pore size. In addition, it is observed that the influence of the pore size on the nonlinear large-amplitude vibration of micro/nano-beam with higher thickness is more prominent.

Figures 7, 8 illustrate, respectively, the effects of nonlocality and strain gradient size dependence on the nonlinear frequency-deflection response of micro/nano-beams made of nanoporous material corresponding to various pore sizes. It is supposed that $L = 500nm$. It is revealed that, for all pore sizes, by increasing the maximum deflection of the micro/nano-beam, both types of size effect diminishes, so the gap between the size-dependent and size-independent frequency-deflection curves decreases.

In Tables 1 and 2, the size-dependent nonlinear frequency of micro/nano-beams made of nanoporous material with different pore sizes are given corresponding to various nonlocal and strain gradient parameters, respectively. The percentages given in parentheses indicate the amount of the reduction or increment in nonlinear frequency due to the size effect. It is found that, by increasing the maximum deflection, both types of size dependence in the nonlinear frequency of micro/nano-beam reduce, as for the linear frequency ($W_{max} = 0$), the size effects are the maximum for all the pore sizes. Moreover, it can be observed that, for all values of maximum deflection and pore sizes, the strain gradient size effect has more effect than nonlocality on the nonlinear frequency of micro/nano-beam made of nanoporous material, as for the same small-scale parameter, the percentage associated with the strain gradient size effect is more than that of nonlocal one.

6 Concluding remarks

In this paper, the size-dependent nonlinear large-amplitude vibrations of micro/nano-beams made of nanoporous material was studied. To accomplish this end, first, refined truncated cube cells were defined to model the porosity of

Table 1 Size-dependent nonlinear frequency (MHz) of micro/nano-beams made of nanoporous material corresponding to different nonlocal parameters and pore sizes ($h = b = 10\text{nm}, L = 500\text{nm}, \text{and} l = 0\mu\text{m}$)

μ(μm)	$\ell/r = 10$	$\ell/r = 20$	$\ell/r = 30$
$W_{\max} = 0$			
0	14.3149	7.0539	4.6892
0.02	14.2032 (−0.780%)	6.9988 (−0.780%)	4.6526 (−0.780%)
0.04	13.8831 (−3.016%)	6.8411 (−3.016%)	4.5478 (−3.016%)
0.06	13.3946 (−6.429%)	6.6004 (−6.429%)	4.3877 (−6.429%)
0.08	12.7900 (−10.652%)	6.3025 (−10.652%)	4.1897 (−10.652%)
0.1	12.1209 (−15.327%)	5.9727 (−15.327%)	3.9705 (−15.327%)
$W_{\max} = 0.005$			
0	22.1210	10.9004	7.2463
0.02	22.0489 (−0.326%)	10.8649 (−0.326%)	7.2226 (−0.326%)
0.04	21.8441 (−1.252%)	10.7640 (−1.252%)	7.1556 (−1.252%)
0.06	21.5369 (−2.641%)	10.6126 (−2.641%)	7.0549 (−2.641%)
0.08	21.1661 (−4.317%)	10.4299 (−4.317%)	6.9335 (−4.317%)
0.1	20.7686 (−6.114%)	10.2340 (−6.114%)	6.8033 (−6.114%)
$W_{\max} = 0.01$			
0	36.6417	18.0557	12.0029
0.02	36.5982 (−0.119%)	18.0342 (−0.119%)	11.9886 (−0.119%)
0.04	36.4751 (−0.455%)	17.9736 (−0.455%)	11.9483 (−0.455%)
0.06	36.2919 (−0.955%)	17.8833 (−0.955%)	11.8883 (−0.955%)
0.08	36.0731 (−1.552%)	17.7755 (−1.552%)	11.8166 (−1.552%)
0.1	35.8412 (−2.185%)	17.6612 (−2.185%)	11.7406 (−2.185%)

Table 2 Size-dependent nonlinear frequency (MHz) of micro/nano-beams made of nanoporous material corresponding to different strain gradient parameters and pore sizes ($h = b = 10\text{nm}, L = 500\text{nm}, \text{and} \mu = 0\mu\text{m}$)

l(μm)	$\ell/r = 10$	$\ell/r = 20$	$\ell/r = 30$
$W_{\max} = 0$			
0	14.3149	7.0539	4.6892
0.02	14.4275 (+0.787%)	7.1093 (+0.787%)	4.7261 (+0.787%)
0.04	14.7601 (+3.110%)	7.2732 (+3.110%)	4.8350 (+3.110%)
0.06	15.2983 (+6.870%)	7.5385 (+6.870%)	5.0113 (+6.870%)
0.08	16.0216 (+11.922%)	7.8948 (+11.922%)	5.2482 (+11.922%)
0.1	16.9060 (+18.101%)	8.3307 (+18.101%)	5.5380 (+18.101%)
$W_{\max} = 0.005$			
0	22.1210	10.9004	7.2463
0.02	22.1941 (+0.330%)	10.9364 (+0.330%)	7.2702 (+0.330%)
0.04	22.4117 (+1.314%)	11.0437 (+1.314%)	7.3415 (+1.314%)
0.06	22.7698 (+2.933%)	11.2202 (+2.933%)	7.4588 (+2.933%)
0.08	23.2620 (+5.158%)	11.4627 (+5.158%)	7.6200 (+5.158%)
0.1	23.8798 (+7.951%)	11.7671 (+7.951%)	7.8224 (+7.951%)
$W_{\max} = 0.01$			
0	36.6417	18.0557	12.0029
0.02	36.6858 (+0.121%)	18.0774 (+0.121%)	12.0173 (+0.121%)
0.04	36.8179 (+0.481%)	18.1425 (+0.481%)	12.0606 (+0.481%)
0.06	37.0371 (+1.079%)	18.2505 (+1.079%)	12.1324 (+1.079%)
0.08	37.3417 (+1.911%)	18.4007 (+1.911%)	12.2322 (+1.911%)
0.1	37.7298 (+2.970%)	18.5919 (+2.970%)	12.3593 (+2.970%)

material. An analytical approach was utilized to extract the mechanical properties of the nanoporous material explicitly in terms of pore size. Afterwards, the nonlocal strain gradient elasticity theory was incorporated to the hyperbolic shear deformable beam theory to construct a refined size-dependent beam model. The Galerkin method together with an improved perturbation technique was employed to propose the analytical expression for nonlocal strain gradient frequency-deflection response of micro/nano-beams made of nanoporous materials with different pore sizes.

It was found that, by increasing the maximum deflection of micro/nano-beam, both types of size dependence have more significant effect on the frequency ratio ($\omega_{\mathrm{NL}}/\omega_{\mathrm{L}}$), especially for lower beam thickness. Furthermore, it was indicated that, by increasing the pore size, the nonlinear frequency of large-amplitude vibration of micro/nano-beams made of nanoporous biomaterial reduces, but the rate of this reduction becomes lower for higher pore size. In addition, it was seen that the influence of the pore size on the nonlinear large-amplitude vibration of micro/nano-beam with higher thickness is more prominent. In addition, it was demonstrated that for all pore sizes, by increasing the maximum deflection of the micro/nano-beam, both types of size effect diminish. Moreover, it was displayed that, for all values of maximum deflection and pore sizes, the strain gradient size effect has more effect than nonlocality on the nonlinear frequency of micro/nano-beam made of nanoporous material.

Appendix

$$S_{11}=\frac{2\,\overline{\overline{AE}}}{\ell},S_{21}=-\frac{2\,\overline{\overline{AE}}}{\ell},S_{31}=S_{41}=S_{51}=S_{61}=0$$

$$S_{12}=-\frac{2\,\overline{\overline{AE}}}{\ell},S_{42}=S_{62}=0$$

$$S_{22}=\frac{4\,\overline{\overline{AE}}}{\ell}+\frac{1}{\frac{\ell^3}{24\overline{\overline{EI}}}+\frac{3\ell}{10\overline{\overline{GA}}}+\frac{3}{5\overline{\overline{GA}}}\left(\frac{\left(1+\frac{\vartheta\ell}{2}\right)cosh(\vartheta\ell)-\left(1+\frac{\vartheta\ell}{2}\right)sinh(\vartheta\ell)-1}{\vartheta}\right)}$$

$$S_{32}=-\frac{2\,\overline{\overline{AE}}}{\ell}-\frac{1}{\frac{\ell^3}{24\overline{\overline{EI}}}+\frac{3\ell}{10\overline{\overline{GA}}}+\frac{3}{5\overline{\overline{GA}}}\left(\frac{\left(1+\frac{\vartheta\ell}{2}\right)cosh(\vartheta\ell)-\left(1+\frac{\vartheta\ell}{2}\right)sinh(\vartheta\ell)-1}{\vartheta}\right)}$$

$$S_{52}=-\frac{2\,\overline{\overline{AE}}}{\ell}+\frac{1}{\frac{\ell^3}{24\overline{\overline{EI}}}+\frac{3\ell}{10\overline{\overline{GA}}}+\frac{3}{5\overline{\overline{GA}}}\left(\frac{\left(1+\frac{\vartheta\ell}{2}\right)cosh(\vartheta\ell)-\left(1+\frac{\vartheta\ell}{2}\right)sinh(\vartheta\ell)-1}{\vartheta}\right)}$$

$$S_{13}=S_{53}=S_{63}=0$$

$$S_{23}=S_{43}=\frac{2\,\overline{\overline{AE}}}{\ell}-\frac{1}{\frac{\ell^3}{24\overline{\overline{EI}}}+\frac{3\ell}{10\overline{\overline{GA}}}+\frac{3}{5\overline{\overline{GA}}}\left(\frac{\left(1+\frac{\vartheta\ell}{2}\right)cosh(\vartheta\ell)-\left(1+\frac{\vartheta\ell}{2}\right)sinh(\vartheta\ell)-1}{\vartheta}\right)}$$

$$S_{33}=\frac{4\,\overline{\overline{AE}}}{\ell}+\frac{1}{\frac{\ell^3}{48\overline{\overline{EI}}}+\frac{3\ell}{20\overline{\overline{GA}}}+\frac{3}{10\overline{\overline{GA}}}\left(\frac{\left(1+\frac{\vartheta\ell}{2}\right)cosh(\vartheta\ell)-\left(1+\frac{\vartheta\ell}{2}\right)sinh(\vartheta\ell)-1}{\vartheta}\right)}$$

$$S_{14}=S_{24}=S_{64}=0$$

$$S_{34}=-\frac{2\,\overline{\overline{AE}}}{\ell}-\frac{1}{\frac{\ell^3}{24\overline{\overline{EI}}}+\frac{3\ell}{10\overline{\overline{GA}}}+\frac{3}{5\overline{\overline{GA}}}\left(\frac{\left(1+\frac{\vartheta\ell}{2}\right)cosh(\vartheta\ell)-\left(1+\frac{\vartheta\ell}{2}\right)sinh(\vartheta\ell)-1}{\vartheta}\right)}$$

$$S_{44}=\frac{4\,\overline{\overline{AE}}}{\ell}+\frac{1}{\frac{\ell^3}{24\overline{\overline{EI}}}+\frac{3\ell}{10\overline{\overline{GA}}}+\frac{3}{5\overline{\overline{GA}}}\left(\frac{\left(1+\frac{\vartheta\ell}{2}\right)cosh(\vartheta\ell)-\left(1+\frac{\vartheta\ell}{2}\right)sinh(\vartheta\ell)-1}{\vartheta}\right)}$$

$$S_{54}=\frac{4\,\overline{\overline{AE}}}{\ell}+\frac{1}{\frac{\ell^3}{24\overline{\overline{EI}}}+\frac{3\ell}{10\overline{\overline{GA}}}+\frac{3}{5\overline{\overline{GA}}}\left(\frac{\left(1+\frac{\vartheta\ell}{2}\right)cosh(\vartheta\ell)-\left(1+\frac{\vartheta\ell}{2}\right)sinh(\vartheta\ell)-1}{\vartheta}\right)}$$

$$S_{15}=S_{35}=0$$

$$S_{25}=-\frac{2\,\overline{\overline{AE}}}{\ell}+\frac{1}{\frac{\ell^3}{24\overline{\overline{EI}}}+\frac{3\ell}{10\overline{\overline{GA}}}+\frac{3}{5\overline{\overline{GA}}}\left(\frac{\left(1+\frac{\vartheta\ell}{2}\right)cosh(\vartheta\ell)-\left(1+\frac{\vartheta\ell}{2}\right)sinh(\vartheta\ell)-1}{\vartheta}\right)}$$

$$S_{45}=\frac{2\,\overline{\overline{AE}}}{\ell}-\frac{1}{\frac{\ell^3}{24\overline{\overline{EI}}}+\frac{3\ell}{10\overline{\overline{GA}}}+\frac{3}{5\overline{\overline{GA}}}\left(\frac{\left(1+\frac{\vartheta\ell}{2}\right)cosh(\vartheta\ell)-\left(1+\frac{\vartheta\ell}{2}\right)sinh(\vartheta\ell)-1}{\vartheta}\right)}$$

$$S_{55}=\frac{20\,\overline{\overline{AE}}}{\ell}+\frac{1}{\frac{\ell^3}{48\overline{\overline{EI}}}+\frac{3\ell}{20\overline{\overline{GA}}}+\frac{3}{10\overline{\overline{GA}}}\left(\frac{\left(1+\frac{\vartheta\ell}{2}\right)cosh(\vartheta\ell)-\left(1+\frac{\vartheta\ell}{2}\right)sinh(\vartheta\ell)-1}{\vartheta}\right)}$$

$$S_{65}=-\frac{8\,\overline{\overline{AE}}}{\ell},\qquad S_{16}=S_{26}=S_{36}=S_{46}=0,$$

$$S_{56}=-\frac{8\,\overline{\overline{AE}}}{\ell},\qquad S_{66}=\frac{8\,\overline{\overline{AE}}}{\ell}.$$

References

1. Shariful Islam M, Todo M (2016) Effects of sintering temperature on the compressive mechanical properties of collagen/hydroxyapatite composite scaffolds for bone tissue engineering. Mater Lett 173:231–234
2. Hedayati R, Amin Yavari S, Zadpoor AA (2017) Fatigue crack propagation in additively manufactured porous biomaterials. Mater Sci Eng C 76:457–463
3. Zhang Y, Li W-Y, Lan R, Wang J-Y (2017) Quality monitoring of porous zein scaffolds: a novel biomaterial. Engineering 3:130–135
4. Bobbert FSL, Lietaert K, Eftekhari AA, Pouran B, Ahmadi SM, Weinans H, Zadpoor AA (2017) Additively manufactured metallic porous biomaterials based on minimal surfaces: a unique combination of topological, mechanical, and mass transport properties. Acta Biomater 53:572–584
5. Kadkhodapour J, Montazerian H, Darabi ACh, Zargarian A, Schmauder S (2017) The relationships between deformation mechanisms and mechanical properties of additively manufactured porous biomaterials. J Mech Behav Biomed Mater 70:28–42
6. Beg S, Rahman M, Jain A, Saini S, Midoux P et al (2017) Nanoporous metal organic frameworks as hybrid polymer–metal composites for drug delivery and biomedical applications. Drug Discov Today 22:625–637
7. Xu X-J, Deng Z-C (2013) Surface effects of adsorption-induced resonance analysis of micro/nanobeams via nonlocal elasticity. Appl Math Mech 34:37–44
8. Farrokhabadi A, Koochi A, Kazemi A, Abadyan M (2014) Effects of size-dependent elasticity on stability of nanotweezers. Appl Math Mech 35:1573–1590
9. Sahmani S, Bahrami M, Ansari R (2014) Nonlinear free vibration analysis of functionally graded third-order shear deformable microbeams based on the modified strain gradient elasticity theory. Compos Struct 110:219–230
10. Li L, Hu Y (2015) Buckling analysis of size-dependent nonlinear beams based on a nonlocal strain gradient theory. Int J Eng Sci 97:84–94
11. Sahmani S, Bahrami M, Aghdam MM, Ansari R (2015) Postbuckling behavior of circular higher-order shear deformable nanoplates including surface energy effects. Appl Math Model 39:3678–3689
12. Ghorbanpour Arani A, Abdollahian M, Jalaei MH (2015) Vibration of bioliquid-filled microtubules embedded in cytoplasm including surface effects using modified couple stress theory. J Theor Biol 367:29–38
13. Yu YJ, Xue Z-N, Li C-L, Tian X-G (2016) Buckling of nanobeams under nonuniform temperature based on nonlocal thermoelasticity. Compos Struct 146:108–113
14. Simsek M (2016) Nonlinear free vibration of a functionally graded nanobeam using nonlocal strain gradient theory and a novel Hamiltonian approach. Int J Eng Sci 105:12–27
15. Sahmani S, Aghdam MM, Akbarzadeh AH (2016) Size-dependent buckling and postbuckling behavior of piezoelectric cylindrical nanoshells subjected to compression and electrical load. Mater Des 105:341–351
16. Wang Y-Z, Wang T-S, Ke L-L (2016) Nonlinear vibration of carbon nanotube embedded in viscous elastic matrix under parametric excitation by nonlocal continuum theory. Physica E 83:195–200
17. Tang Y, Liu Y, Zhao D (2016) Viscoelastic wave propagation in the viscoelastic single walled carbon nanotubes based on nonlocal strain gradient theory. Physica E 84:202–208
18. Sahmani S, Aghdam MM (2017) Temperature-dependent nonlocal instability of hybrid FGM exponential shear deformable nanoshells including imperfection sensitivity. Int J Mech Sci 122:129–142
19. Sahmani S, Aghdam MM (2017) Size dependency in axial postbuckling behavior of hybrid FGM exponential shear deformable nanoshells based on the nonlocal elasticity theory. Compos Struct 166:104–113
20. Sahmani S, Aghdam MM (2017) Nonlinear instability of hydrostatic pressurized hybrid FGM exponential shear deformable nanoshells based on nonlocal continuum elasticity. Compos Part B Eng 114:404–417
21. Rajasekaran S (2018) Analysis of axially functionally graded nano-tapered Timoshenko beams by element-based Bernstein pseudospectral collocation (EBBPC). Eng Comput 34:543–563
22. Yang Z, He D (2017) Vibration and buckling of orthotropic functionally graded micro-plates on the basis of a re-modified couple stress theory. Results Phys 7:3778–3787
23. Sahmani S, Fattahi AM (2017) Nonlocal size dependency in nonlinear instability of axially loaded exponential shear deformable FG-CNT reinforced nanoshells under heat conduction. Eur Phys J Plus 132:231
24. Sahmani S, Fattahi AM (2017) An anisotropic calibrated nonlocal plate model for biaxial instability analysis of 3D metallic carbon nanosheets using molecular dynamics simulations. Mater Res Express 4:065001
25. Sahmani S, Fattahi AM (2017) Size-dependent nonlinear instability of shear deformable cylindrical nanopanels subjected to axial compression in thermal environments. Microsyst Technol 23:4717–4731
26. He D, Yang W, Chen W (2017) A size-dependent composite laminated skew plate model based on a new modified couple stress theory. Acta Mech Solida Sin 30:75–86
27. Mirsalehi M, Azhari M, Amoushahi H (2017) Buckling and free vibration of the FGM thin micro-plate based on the modified strain gradient theory and the spline finite strip method. Eur J Mech A Solids 61:1–13
28. Sahmani S, Fattahi AM (2017) Thermo-electro-mechanical size-dependent postbuckling response of axially loaded piezoelectric shear deformable nanoshells via nonlocal elasticity theory. Microsyst Technol 23:5105–5119
29. Sahmani S, Aghdam MM (2017) Imperfection sensitivity of the size-dependent postbuckling response of pressurized FGM nanoshells in thermal environments. Arch Civ Mech Eng 17:623–638
30. Kheibari F, Tadi Y (2017) Beni. Size dependent electro-mechanical vibration of single-walled piezoelectric nanotubes using thin shell model. Mater Des 114:572–583
31. Radic N, Jeremic D (2017) A comprehensive study on vibration and buckling of orthotropic double-layered graphene sheets under hygrothermal loading with different boundary conditions. Compos Part B Eng 128:182–199
32. Fattahi AM, Sahmani S (2017) Size dependency in the axial postbuckling behavior of nanopanels made of functionally graded material considering surface elasticity. Arab J Sci Eng 42:4617–4633
33. Chen X, Li Y (2018) Size-dependent post-buckling behaviors of geometrically imperfect microbeams. Mech Res Commun 88:25–33
34. Trinh LC, Vo TP, Thai H-T, Nguyen T-K, Keerthan P (2018) State-space Levy solution for size-dependent static, free vibration and buckling behaviours of functionally graded sandwich plates. Compos Part B Eng 149:144–164
35. Sahmani S, Aghdam MM (2018) Nonlocal electrothermomechanical instability of temperature-dependent FGM nanopanels with piezoelectric facesheets. Iran J Sci Technol Trans Mech Eng. https://doi.org/10.1007/s40997-018-0180-y
36. Sahmani S, Fattahi AM, Ahmed NA (2018) Nonlinear torsional buckling and postbuckling analysis of cylindrical silicon

nanoshells incorporating surface free energy effects. Microsyst Technol. https://doi.org/10.1007/s00542-018-4246-y
37. Li L, Tang H, Hu Y (2018) The effect of thickness on the mechanics of nanobeams. Int J Eng Sci 123:81–91
38. Kim J, Kamil Zur K, Reddy JN (2019) Bending, free vibration, and buckling of modified couples stress-based functionally graded porous micro-plates. Compos Struct 209:879–888
39. Chen X, Lu Y, Li Y (2019) Free vibration, buckling and dynamic stability of bi-directional FG microbeam with a variable length scale parameter embedded in elastic medium. Appl Math Model 67:430–448
40. Sarafraz A, Sahmani S, Aghdam MM (2019) Nonlinear secondary resonance of nanobeams under subharmonic and superharmonic excitations including surface free energy effects. Appl Math Model 66:195–226
41. Zhu X, Li L (2017) Closed form solution for a nonlocal strain gradient rod in tension. Int J Eng Sci 119:16–28
42. Zhu X, Li L (2017) On longitudinal dynamics of nanorods. Int J Eng Sci 120:129–145
43. Lim CW, Zhang G, Reddy JN (2015) A higher-order nonlocal elasticity and strain gradient theory and its applications in wave propagation. J Mech Phys Solids 78:298–313
44. Li L, Hu Y (2016) Wave propagation in fluid-conveying viscoelastic carbon nanotubes based on nonlocal strain gradient theory. Comput Mater Sci 112:282–288
45. Li L, Li X, Hu Y (2016) Free vibration analysis of nonlocal strain gradient beams made of functionally graded material. Int J Eng Sci 102:77–92
46. Yang WD, Yang FP, Wang X (2016) Coupling influences of nonlocal stress and strain gradient on dynamic pull-in of functionally graded nanotubes reinforced nano-actuator with damping effects. Sens Actuators A Phys 248:10–21
47. Li L, Hu Y, Li X (2016) Longitudinal vibration of size-dependent rods via nonlocal strain gradient theory. Int J Mech Sci 115 –116 135–144
48. Sahmani S, Aghdam MM (2017) Nonlinear instability of axially loaded functionally graded multilayer graphene platelet-reinforced nanoshells based on nonlocal strain gradient elasticity theory. Int J Mech Sci 131:95–106
49. Sahmani S, Aghdam MM (2017) A nonlocal strain gradient hyperbolic shear deformable shell model for radial postbuckling analysis of functionally graded multilayer GPLRC nanoshells. Compos Struct 178:97–109
50. Sahmani S, Aghdam MM (2017) Nonlocal strain gradient beam model for nonlinear vibration of prebuckled and postbuckled multilayer functionally graded GPLRC nanobeams. Compos Struct 179:77–88
51. Sahmani S, Aghdam MM (2017) Axial postbuckling analysis of multilayer functionally graded composite nanoplates reinforced with GPLs based on nonlocal strain gradient theory. Eur Phys J Plus 132:490
52. Li L, Hu Y (2017) Post-buckling analysis of functionally graded nanobeams incorporating nonlocal stress and microstructure-dependent strain gradient effects. Int J Mech Sci 120:159–170
53. Xu X-J, Wang X-C, Zheng M-L, Ma Z (2017) Bending and buckling of nonlocal strain gradient elastic beams. Compos Struct 160:366–377
54. Shahsavari D, Karami B, Li L (2018) Damped vibration of a graphene sheet using a higher-order nonlocal strain-gradient Kirchhoff plate model. Comptes Rendus Mecanique 346:1216–1232
55. Sahmani S, Aghdam MM (2017) Size-dependent axial instability of microtubules surrounded by cytoplasm of a living cell based on nonlocal strain gradient elasticity theory. J Theor Biol 422:59–71
56. Sahmani S, Aghdam MM (2017) Nonlinear vibrations of pre-and post-buckled lipid supramolecular micro/nano-tubules via nonlocal strain gradient elasticity theory. J Biomech 65:49–60
57. Sahmani S, Aghdam MM (2018) Nonlocal strain gradient beam model for postbuckling and associated vibrational response of lipid supramolecular protein micro/nano-tubules. Math Biosci 295:24–35
58. Sahmani S, Aghdam MM (2018) Nonlinear instability of hydrostatic pressurized microtubules surrounded by cytoplasm of a living cell including nonlocality and strain gradient microsize dependency. Acta Mech 229:403–420
59. Lu L, Guo X, Zhao J (2017) Size-dependent vibration analysis of nanobeams based on the nonlocal strain gradient theory. Int J Eng Sci 116:12–24
60. Radic N (2018) On buckling of porous double-layered FG nanoplates in the Pasternak elastic foundation based on nonlocal strain gradient elasticity. Compos Part B Eng 153:465–479
61. Sahmani S, Aghdam MM, Rabczuk T (2018) Nonlinear bending of functionally graded porous micro/nano-beams reinforced with graphene platelets based upon nonlocal strain gradient theory. Compos Struct 186:68–78
62. Sahmani S, Aghdam MM, Rabczuk T (2018) A unified nonlocal strain gradient plate model for nonlinear axial instability of functionally graded porous micro/nano-plates reinforced with graphene platelets. Mater Res Express 5:045048
63. Sahmani S, Aghdam MM, Rabczuk T (2018) Nonlocal strain gradient plate model for nonlinear large-amplitude vibrations of functionally graded porous micro/nano-plates reinforced with GPLs. Compos Struct 198:51–62
64. Zhen Y-X, Wen S-L, Tang Y (2019) Free vibration analysis of viscoelastic nanotubes under longitudinal magnetic field based on nonlocal strain gradient Timoshenko beam model. Physica E 105:116–124
65. Sahmani S, Khandan A (2018) Size dependency in nonlinear instability of smart magneto-electro-elastic cylindrical composite nanopanels based upon nonlocal strain gradient elasticity. Microsyst Technol. https://doi.org/10.1007/s00542-018-4072-2
66. Sahmani S, Fattahi AM, Ahmed NA (2018) Analytical mathematical solution for vibrational response of postbuckled laminated FG-GPLRC nonlocal strain gradient micro-/nanobeams. Eng Comput https://doi.org/10.1007/s00366-018-0657-8
67. Lu L, Guo X, Zhao J (2019) A unified size-dependent plate model based on nonlocal strain gradient theory including surface effects. Appl Math Model 68:583–602
68. Esfahani S, Esmaeilzade Khadem S, Ebrahimi A, Mamaghani (2019) Nonlinear vibration analysis of an electrostatic functionally graded nano-resonator with surface effects based on nonlocal strain gradient theory. Int J Mech Sci 151:508–522
69. Hedayati R, Sadighi M, Aghdam MM, Zadpoor AA (2017) Analytical relationships for the mechanical properties of additively manufactured porous biomaterials based on octahedral unit cells. Appl Math Model 46:408–422
70. Shen H-S, Yang D-Q (2015) Nonlinear vibration of functionally graded fiber reinforced composite laminated beams with piezoelectric fiber reinforced composite actuators in thermal environments. Eng Struct 90:183–192
71. Shen H-S, Chen X, Huang X-L (2016) Nonlinear bending and thermal postbuckling of functionally graded fiber reinforced composite laminated beams with piezoelectric fiber reinforced composite actuators. Compos Part B Eng 90:326–335
72. Sahmani S, Bahrami M, Aghdam MM (2016) Surface stress effects on the nonlinear postbuckling characteristics of geometrically imperfect cylindrical nanoshells subjected to axial compression. Int J Eng Sci 99:92–106
73. Sahmani S, Shahali M, Khandan A, Saber-Samandari S, Aghdam MM (2018) Analytical and experimental analyses for mechanical and biological characteristics of novel nanoclay bio-nanocomposite scaffolds fabricated via space holder technique. Appl Clay Sci 165:112–123

74. Shen H-S, Xiang Y (2018) Postbuckling of functionally graded graphene-reinforced composite laminated cylindrical shells subjected to external pressure in thermal environments. Thin Walled Struct 124:151–160
75. Sahmani S, Saber-Samandari S, Shahali M, Yekta HJ et al (2018) Mechanical and biological performance of axially loaded novel bio-nanocomposite sandwich plate-type implant coated by biological polymer thin film. J Mech Behav Biomed Mater 88:238–250
76. Sahmani S, Saber-Samandari S, Aghdam MM, Khandan A (2018) Nonlinear resonance response of porous beam-type implants corresponding to various morphology shapes for bone tissue engineering applications. J Mater Eng Perform 27:5370–5383
77. Shen H-S, Xiang Y (2018) Postbuckling behavior of functionally graded graphene-reinforced composite laminated cylindrical shells under axial compression in thermal environments. Comput Methods Appl Mech Eng 330:64–82
78. Sahmani S, Aghdam MM (2018) Nonlinear size-dependent instability of hybrid FGM nanoshells. In: Dai L, Jazar R (eds) Nonlinear approaches in engineering applications. Springer, Cham, pp 107–143
79. Sahmani S, Aghdam MM (2018) Boundary layer modeling of nonlinear axial buckling behavior of functionally graded cylindrical nanoshells based on the surface elasticity theory. Iran J Sci Technol Trans Mech Eng 42:229–245
80. Wang Z-X, Shen H-S (2018) Nonlinear vibration of sandwich plates with FG-GRC face sheets in thermal environments. Compos Struct 192:642–653
81. Sahmani S, Saber-Samandari S, Khandan A, Aghdam MM (2019) Nonlinear resonance investigation of nanoclay based bio-nanocomposite scaffolds with enhanced properties for bone substitute applications. J Alloy Compd 773:636–653
82. Fan Y, Xiang Y, Shen H-S (2019) Nonlinear forced vibration of FG-GRC laminated plates resting on visco-Pasternak foundations. Compos Struct 209:443–452
83. Ahmadi SM, Campoli G, Amin Yavari S, Sajadi B et al (2014) Mechanical behavior of regular open-cell porous biomaterials made of diamond lattice unit cells. J Mech Behav Biomed Mater 34:106–115